BJR

BONE FRACTURE

microRNA-136-5p from bone marrow mesenchymal stem cell-derived exosomes facilitates fracture healing by targeting LRP4 to activate the Wnt/β-catenin pathway

H. Yu,
J. Zhang,
X. Liu,
Y. Li

From The Second Hospital of Jilin University, Changchun, China

Aims

Exosomes derived from bone marrow mesenchymal stem cells (BMSCs) have been reported to be a promising cellular therapeutic approach for various human diseases. The current study aimed to investigate the mechanism of BMSC-derived exosomes carrying microRNA (miR)-136-5p in fracture healing.

Methods

A mouse fracture model was initially established by surgical means. Exosomes were isolated from BMSCs from mice. The endocytosis of the mouse osteoblast MC3T3-E1 cell line was analyzed. CCK-8 and disodium phenyl phosphate microplate methods were employed to detect cell proliferation and alkaline phosphatase (ALP) activity, respectively. The binding of miR-136-5p to low-density lipoprotein receptor related protein 4 (LRP4) was analyzed by dual luciferase reporter gene assay. HE staining, tartrate-resistant acid phosphatase (TRAP) staining, and immunohistochemistry were performed to evaluate the healing of the bone tissue ends, the positive number of osteoclasts, and the positive expression of β-catenin protein, respectively.

Results

miR-136-5p promoted fracture healing and osteoblast proliferation and differentiation. BMSC-derived exosomes exhibited an enriched miR-136-5p level, and were internalized by MC3T3-E1 cells. LRP4 was identified as a downstream target gene of miR-136-5p. Moreover, miR-136-5p or exosomes isolated from BMSCs (BMSC-Exos) containing miR-136-5p activated the Wnt/β-catenin pathway through the inhibition of LRP4 expression. Furthermore, BMSC-derived exosomes carrying miR-136-5p promoted osteoblast proliferation and differentiation, thereby promoting fracture healing.

Conclusion

BMSC-derived exosomes carrying miR-136-5p inhibited LRP4 and activated the Wnt/β-catenin pathway, thus facilitating fracture healing.

Cite this article: *Bone Joint Res* 2021;10(12):744–758.

Keywords: Bone marrow mesenchymal stem cells, Exosomes, miR-136-5p

Article focus

- Mechanism by which bone marrow mesenchymal stem cell (BMSC) exosomes carrying miR-136-5p facilitate fracture healing.

Key messages

- microRNA (miR)-136-5p promotes fracture healing, osteoblast proliferation, and differentiation, both in vivo and in vitro.
- miR-136-5p-containing BMSC-Exospromote osteoblast proliferation and differentiation, thereby promoting fracture healing.

Strengths and limitations

- The paracrine transfer of miRs presents a promising novel approach towards miR-based therapy in fracture healing.

Correspondence should be sent to Yingzhi Li; email: dlyz2005@jlu.edu.cn

doi: 10.1302/2046-3758.1012.BJR-2020-0275.R2

Bone Joint Res 2021;10(12):744–758.

- The unclear clinical application is a limitation.

Introduction

The incidence of life-threatening fractures of long bones has increased dramatically as a consequence of the increase in motor transport, particularly in developing countries.[1] Bone fractures are under-investigated injuries, with little known about their frequency, risk factors, and locations, in spite of their debilitating consequences that impede the rehabilitation.[2] Thus, a deeper understanding of the mechanisms underpinning the process of fracture healing is crucial for avoiding post-fracture adverse events. Fortunately, unlike other tissues, bones display a significant capacity for healing, a complex and multistep process involving various genes and other molecules.[3,4]

Exosomes, containing various entities including lipids, nucleic acids, proteins, and signalling molecules,[5] were initially discovered as exfoliated membrane vesicles in 1981.[6] More recently, exosomes have been defined as cellular organelles that are released by various tissues or cells and can be taken up by recipient cells via endocytosis.[7] Recent evidence has been presented demonstrating the ability of exosomes to stimulate the regeneration and repair of tissue and organs.[8] Moreover, endocytosis of exosomes can facilitate the absorption of proteins, messenger RNAs (mRNAs), and microRNAs (miRNAs or miRs), thereby affecting target cells.[9] Moreover, bone marrow mesenchymal stem cells (BMSCs) represent an optimal progenitor cell source that plays a role in facilitating bone repair. The current study aimed to elucidate the role of exosomes derived from BMSCs in bone fracture healing.

miRNAs represent a class of noncoding RNAs modulating gene expression on a post-transcriptional level, and have been implicated in various biological processes such as stem cell self-renewal and metabolism.[10] Accumulating evidence continues to highlight the potential of molecular therapy using miRNAs as a treatment for impaired fracture healing due to their differential expression patterns.[11] Through base pairing in the 3'-untranslated region (3'-UTR) of target mRNAs, miRNAs commonly suppress the expression of their targets.[12] In addition to the activity of miRNAs reported in MSCs, osteoblasts, or osteoclasts,[13,14] the role of miRNAs has been further implicated in the process of osteogenic differentiation, such as inhibiting MSC differentiation into osteoblasts.[15,16]

Members of the low-density lipoprotein receptor-related protein (LRP) gene family, especially lipoprotein-related protein 4 (LRP4), have been reported to play a role in the physiology of bone via the Wnt/β-catenin (Wnt) signalling pathway.[17] The Wnt pathway represents a topic of particular research interest with studies highlighting its role in various physiological processes and crucial activity in bone development, as well as bone healing and regeneration following injury.[18] Wnt ligands can accelerate bone growth and thus indicate the potential fracture healing-promoting effects of the Wnt pathway.[19]

Hence, based on the exploration of the aforementioned literature, we set out to elucidate the role of BMSC-derived exosomes in bone fracture healing with an emphasis on relevant functional miRNAs and common signalling pathways, such as the Wnt pathway.

Methods

Ethics statement. All animal experiments were performed with the approval of the Animal Ethics Committee of our hospital and in strict adherence with the Guide for the Care and Use of Laboratory Animals published by the USA National Institutes of Health. Extensive efforts were made to ensure minimal animal suffering and number of animals included in the experiments.

Establishment of mouse fracture models. Male C57BL/6 J mice, aged seven to ten weeks with body weight around 19.66 g (standard deviation (SD) 2.21), were housed in specific pathogen-free (SPF) animal rooms. Fracture models were established using the aforementioned mice following an acclimation period of two weeks based on previously described methods:[20,21] C-shaped instruments with three-point bending were applied to create transverse femoral fractures. The right knee was exposed via the lateral parapatellar approach, with the medial patella subsequently dislocated. The femoral intercondylar groove was fully flexed and exposed to the knee joint, after which a burr hole with a diameter of 0.5 mm was made in the centre of the intercondylar groove. In order to avoid any significant displacement of the fracture, and to keep the fracture site neat and stable, a 24 mm needle with a diameter of 0.5 mm was inserted into the burr hole in the centre of the intercondylar sulcus. Following minimal lateral exposure, a thin cut 3 mm deep on the central axis was made while avoiding complex fractures. The right femur of each animal was fractured using the aforementioned three-point bending method, after which the muscle fascia and skin were sutured. Finally, micro-CT scan was used to verify successful model establishment.

Regarding tissue preparation, eight weeks after the operation the mice were anaesthetized and whole blood samples were collected through cardiac puncture. After being incubated at room temperature for 30 minutes, the blood samples were centrifuged at 5,000 rpm for ten minutes, and then serum was separated for bone marker detection. The mice were further anaesthetized to death followed with the tibia being removed and fixed overnight. Some specimens were directly buried in plastic, and the rest of the samples were fully decalcified with 10% ethylenediaminetetraacetic acid and made into paraffin-embedded sections.

Experimental animal grouping and treatments. The mice were divided into eight groups: sham group (mice receiving sham operation), model group (fractured mice without further treatment), model+ agomir-negative control (NC) group (fractured mice injected with agomir-NC), model+ miR-136-5p group (fractured mice injected with miR-136-5p agomir), model+ NC-mimic-Exos+

overexpression (oe)-NC group (fractured mice injected with exosomes from NC-mimic-transfected BMSCs and oe-NC plasmids), model+ NC-mimic-Exos+ oe-DKK1 group (fractured mice injected with exosomes from NC-mimic-transfected BMSCs and DKK1 (a Wnt/β-catenin pathway inhibitor) overexpression plasmids), model+ miR-136-5p mimic-Exos+ oe NC group (fractured mice injected with exosomes from miR-136-5p mimic-transfected BMSCs and oe-NC plasmids), and model+ miR-136-5p mimic-Exos+ oe-DKK1 group (fractured mice injected with exosomes from miR-136-5p mimic-transfected BMSCs and DKK1 overexpression plasmids). There were ten mice per group and 80 mice in total.

After the mouse models had been successfully grouped as mentioned previously, the oligonucleotide or plasmids described in each group were diluted with transfection reagent in accordance with the instructions of the animal transfection reagent (En-transter in vivo, Thermo Fisher Scientific, USA), and transferred into mice via tail vein injection once a day for three days. Mice of the Sham and Model groups were injected with 100 µl phosphate-buffered saline once a day for three days. All plasmids, sequencing identification, virus packaging, and titer testing were procured from Genechem (China).

Cell culture. Mouse BMSCs (CP-M131; Procell Life Science&Technology Co., Ltd., China were cultured at 37°C with 5% CO_2. The cells at passage 4 to 6 were collected and seeded into a six-well plate at a density of 1.0 × 10^5 cells/well. The following day, the cells were washed with serum-free Dulbecco's modified Eagle's medium (DMEM) and cultured with serum-free DMEM (2 ml/well) for another 48 hours. No spontaneous differentiation was observed during the cultivation process. As per the instructions of the BMSC osteogenic differentiation (osteogenesis, adipogenesis) kit (CHEM-200004/5/6, Shanghai Linmeng Biotechnology, China), alizarin red S and oil red O staining were performed to observe osteogenic and adipogenic differentiation ability of BMSCs, respectively. Exosome-free serum was purchased from Sun Ran Biotechnology (EXO-FBS-50A-1-SBI; China). Besides, MLO-Y4 (CL-0567, Procell Life Science&Technology Co., Ltd.), a murine long bone-derived osteocyte-like cell line (serving as controls to BMSCs and their exosomes),[22] was stored in DMEM (Wako, Pure Chemical, Japan) containing 10% fetal bovine serum (FBS) and 1% penicillin and streptomycin solution (Nacalai Tesque, Japan).

Mouse osteoblast cell line MC3T3-E1 (CL-0251, Procell Life Science&Technology Co., Ltd.) was cultured in α-minimal medium (Thermo Fisher Scientific, USA) containing 10% FBS (PAA Laboratories, Germany), 1% penicillin/streptomycin (Thermo Fisher Scientific) and 1% l-glutamine (Biochrom, Germany). In order to trigger osteogenic differentiation, 10 mM β-glycerophosphate and 0.2 mM ascorbic acid-2-phosphate (both from Sigma-Aldrich) were added to the culture medium.

Cell grouping and transfection. Cells were seeded (3 × 10^5 cells/ml; 3 ml) into six-well plates upon reaching 80% to 90% confluence. Cell transfection was then conducted using Lipofectamine 2000 (11668-019, Invitrogen, USA) according to protocols provided by the manufacturer.

To examine the effects of exosomes isolated from BMSCs (BMSC-Exos) on osteoblasts, MC3T3-E1 cells were cultured in medium containing BMSC-Exos or PBS or just medium, divided into BMSC-Exos+ MC3T3-E1, PBS + MC3T3-E1, and Culture medium+ MC3T3-E1 groups.

To examine the effects of miR-136-5p on osteoblasts, MC3T3-E1 cells were transfected with plasmids expressing miR-136-5p mimic or inhibitor or corresponding NC, signed as miR-136-5p mimic, NC-mimic, miR-136-5p inhibitor, and NC-inhibitor groups.

To investigate the role of miR-136 to 5 p/LRP4 axis in fracture healing, MC3T3-E1 cells were transfected with the combination of plasmids expressing miR-136-5p mimic/NC-mimic with LRP4/NC overexpression plasmids, signed as NC-mimic+ oe NC, NC-mimic+ oe-LRP4, miR-136-5p mimic+ oe NC, miR-136-5p mimic+ oe-LRP4 groups.

To evaluate the effects of miR-136-5p shuttled by BMSC-Exos on osteoblasts, METTL3 cells transfected with plasmids expressing miR-136-5p inhibitor or NC-inhibitor were cultured in medium containing BMSC-Exos or PBS, signed as BMSC-Exos+ miR-136-5p inhibitor, BMSC-Exos+ NC-inhibitor, and PBS + NC-inhibitor groups.

Further, to investigate the regulatory role of miR-136-5p-carrying BMSC-Exos targeting LRP4 in fracture healing, METTL3 cells transfected with LRP4 or NC overexpression plasmids were cultured with Exos derived from BMSCs expressing miR-136-5p mimic or NC-mimic, divided into BMSC-Exos-miR-136-5p mimic+ oe-LRP4, BMSC-Exos-miR-136-5p mimic+ oe NC, BMSC-Exos-NC mimic+ oe-LRP4, and BMSC-Exos-NC mimic+ oe NC groups. All aforementioned plasmids and sequences were designed and constructed from the pcDNA3.1 vector by Genechem (China).

Isolation and identification of exosomes. After the BMSCs had reached 80% to 90% confluence, the exosomes were separated from the cell culture supernatant by means of ultra-centrifugation: the collected culture supernatant was centrifuged at 500 g for 15 minutes for cell debris removal purposes, followed by further centrifugation at 2,000 g for another 15 minutes to remove both cell debris as well as apoptotic bodies, and finally centrifuged at 10,000 g for 20 minutes to remove large vesicles. After being filtered and centrifuged, the pellet was collected and subsequently resuspended in PBS. The PBS resuspension solution was then further centrifuged at 110,000 g for 70 minutes, and then resuspended again in 100 µl of sterile PBS for future experiments. All ultracentrifugation steps were performed at 4°C using a Beckman (TL-100) ultracentrifuge, TLS-55 swinging bucket rotor. For the rest low-speed centrifugation, a Beckman Allegra X-15R desktop centrifuge (USA) was used. The obtained exosomes were stored at -80°C.

Identification of the cell exosomes by a transmission electron microscopy (TEM): 20 µl of cell exosomes was added in a dropwise manner onto a copper mesh and

rested for three minutes. Next, phosphotungstic acid solution (30 µl, pH = 6.8) was added for counterstaining, followed by TEM observation. Then, the size of exosomes was analyzed by nanoparticle tracking (NS300, Malvern Instruments, UK) and related surface markers were identified by Western blot. The protein content of the exosome suspension was determined with bicinchoninic acid (BCA) kit (23227, Thermo Fisher Scientific) and sodium dodecyl sulfate-polyacrylamide gel electrophoresis (SDS-PAGE) was performed followed by transfer to a membrane. The expression of exosome-specific marker protein was detected with western blot: tumour susceptibility gene 101 (TSG101) (ab30871, 1: 1,000), CD63 (ab68418, 1: 1,000), CD81 (ab109201, 1: 2,000), and GRP94 (ab3674, 1: 3,000). Ponceau red was employed as the loading Sham. The aforementioned antibodies were all from Abcam (Cambridge, UK).

Exosome uptake of cells. The purified BMSC-Exos were labelled with PKH67 Green Fluorescence Kit (PKH67GL-1KT, Sigma-Aldrich) and then were resuspended in 1 ml Diluent C solution, which was added with 4 µl of PKH67 ethanol dye solution for the preparation of dye solution (4×10^{-6} M). Subsequently, Exos suspension (1 ml) was mixed with the dye solution for five minutes and then 2 ml of 1% bovine serum albumin (BSA) was added for one minute of incubation for staining termination purposes, followed by ultracentrifugation, PBS washing, and resuspending.

MC3T3-E1 cells were incubated with PKH67-labelled exosomes at 37°C for 12 hours followed by fixation with 4% paraformaldehyde. The nuclei were subsequently stained using 4',6-diamidino-2-phenylindole (DAPI) and the cell membrane was stained red with Diluent C (C1036, Beyotime Biotechnology, China). A fluorescence microscope (Zeiss LSM 800, Carl Zeiss, Germany) was used to observe and analyze the uptake of Exos labelled by MC3T3-E1.

Uptake of BMSC-Exos carrying Cy3-miR-136-5p by MC3T3-E1: BMSCs were transfected with Cy3-miR-136 to 5 p lentivirus in serum-free medium (GenePharma, China) using lipo3000 kit (Invitrogen, L3000001) for six hours. The culture medium was subsequently replaced by 10% exosome-free serum and cultured for an additional 48 hours. BMSC-Exos from the collected cell supernatant were resuspended with PBS as per the above-mentioned Exos centrifugal step, followed by addition into MC3T3-E1. The cells were then fixed with 4% paraformaldehyde, washed with PBS, and stained in the same manner. A fluorescence microscope (Zeiss, LSM710) was used to observe the uptake of Exos-carrying Cy3-miR-1365p (red light) of MC3T3-E1.

Cell counting kit-8 assay. The cell proliferation ability was detected using CCK-8 kit (CA1210-100, Solarbio, China). Cells exhibiting logarithmic growth were then seeded into 96-well plates (5×10^3 cells/well) for three-day incubation. The testing was initiated after seeding the cells. Upon detection, 10 µl of CCK-8 solution was added into each well and the plate was further incubated for two hours. The optical density (OD) at a wavelength of 450 nm at different timepoints (0 hrs, 24 hrs, 48 hrs, 72 hrs) was measured using a microplate reader (BIO-RAD 680, Bio-Rad Laboratories, USA). Finally, cell proliferation curves were drawn.

Alkaline phosphatase activity measurement. The activity of ALP (bone formation marker) of serum or cell culture supernatant was detected using Disodium phosphate microplate method as per the instructions provided by the manufacturer (G5610, Solarbio). A fully automatic biochemical analyzer (UniCel DxC 800 Synchron Clinical Systems; Beckman Coulter, USA) was used for analysis.

Western blot. The total protein was extracted from cells or tissues using pre-cooled radioimmunoprecipitation assay (RIPA) lysis buffer (R0010, Solarbio) containing phenylmethylsulphonyl fluoride (PMSF) at 4°C. The protein concentration of each sample was then measured using a BCA kit (C503021-0500, Sangon Biotech, China). The sample volumes were adjusted according to their protein concentration, with the total amount of protein for each sample loaded accordingly. After separation using SDS-PAGE, the protein was transferred onto polyvinylidene fluoride (PVDF) membranes (Millipore, USA) via the wet transfer method, followed by blockade with 5% BSA at room temperature for one hour. The membrane was subsequently incubated with the following diluted primary antibodies at 4°C in a shaker overnight: rabbit anti-LRP4 (DF9610, Affinity Biosciences), Wnt4 (ab91226, 1: 1,000), GSK3β (ab3239, 1: 5,000), phosphorylated (p)-GSK3β (Tyr216) (ab75745, 1: 1,000), β-catenin (ab32572, 1: 5,000), p-β-catenin (ab27798, 1: 500), proliferating cell nuclear antigen (PCNA; ab92552, 1: 2,000), Runt-related transcription factor 2 (Runx2; Ab23981, 1: 1,000), osteogenic marker gene osteocalcin (OCN; ab93876, 1: 500), and osteopontin (OPN; ab8448, 1: 1,000). After three Tris-buffered saline Tween-20 (TBST) washes (ten mins for each wash), the membrane was incubated with horseradish peroxidase (HRP)-labelled goat anti-rabbit secondary antibody IgG (ab6721, 1: 5,000) at room temperature for one hour. Following another TBST wash (ten mins × 3), the membrane was developed with HRP substrate ECL luminescent liquid (WBKLS0050; Shanghai Lianshuo Biotechnology, China). Finally, with glyceraldehyde-3-phosphate dehydrogenase (GAPDH) (ab8245, 1: 5,000) employed as the internal reference, the gel imaging analysis system (GIS-500, Beijing Qianming Gene Technology, China) and Image J software (National Institutes of Health, USA) were used to analyze the relative expression of proteins of interest. The aforementioned antibodies were all purchased from Abcam.

Reverse transcription quantitative polymerase chain reaction. All callus tissues were separated, lyophilized with liquid nitrogen, and subsequently ground in a mortar, after which total RNA was extracted from the isolated callus tissues, cells, and exosomes with TRIzol reagents (15596-018, Solarbio) based on the manufacturer's instructions. According to the instructions of miRNA reverse

transcription kit (B532451, Sangon Biotech) and cDNA reverse transcription kit (B532445, Sangon Biotech), cDNA was obtained, after which the gene fragment was amplified in the fluorescence quantitative PCR instrument (ABI ViiA 7, Da An Gene of Sun Yat-Sen University, China) with the miR-136-5p reverse transcription primers purchased from RiboBio (Guangdong, China). The remaining gene primers were synthesized by Dalian Takara (Liaoning, China) (Supplementary Table i), which was analyzed using a fluorescence quantitative PCR kit (AQ101-02, TransGen Biotech, Beijing, China). GAPDH was regarded as an internal reference for the loading control. In regard to the miRNA, U6 served as an internal reference. The relative transcription level of a target gene was calculated using $2^{-\Delta\Delta CT}$ method.

Dual luciferase reporter gene assay. The online website TargetScan[23] was employed to predict the targeting relationship between the 3'-UTR of LRP4 mRNA and miR-136-5p, with a luciferase reporter gene assay used to further verify the predicted results. The dual luciferase reporter gene vector of both the wild type and mutated target gene LRP4 were constructed respectively: pGLO-LRP4-wild type (WT) and pGLO-LRP4-mutant type (MUT) with mutations on the predicted binding site of miR-136-5p. HEK293 cells were cotransfected with either reporter plasmid with miR-136-5p mimic and the internal reference plasmid expressing Renilla luciferase (pRL-TK). At 48 hours post-transfection, the cells were collected, after which a dual luciferase report analysis system (E1910; Promega Corporation, USA) was used to determine the relative luciferase activity. Relative luciferase activity = firefly luciferase activity/renin luciferase activity.

Haematoxylin-eosin staining. The preserved tissue sample section was deparaffinized, stained with haematoxylin for five minutes, and eosin for 15 seconds. Then, the slides were dehydrated and sealed for observation.

Tartrate-resistant acid phosphatase staining. Tissue sections were dewaxed with xylene, hydrated, and incubated at 37°C with tartrate-resistant acid phosphatase (TRAP) staining solution for 30 minutes under conditions void of light. The sections were subsequently stained with methyl green for five minutes and dehydrated with gradient alcohol. The sections were then washed with toluene, and sealed with neutral balsam. All chemical reagents used in this experiment were purchased from Chuandong Chemical Company (Chongqing, China). The section was photographed, with the number of TRAP-positive cells in five random areas counted.

Immunohistochemistry. Paraffin specimens were sliced into 4-μm-thick sections, dewaxed, hydrated, and then immunostained with primary antibody against Wnt4 (ab91226, 1: 200, Abcam) and secondary antibody against IgG (ab150083, 1: 100, Abcam). Non-specific normal IgG was employed as a NC. The staining results were obtained by randomly selecting five lesion areas under 200 or 400 magnifications and counting the number of positively stained cells in the view area. The results were expressed as the positive cell value with standard deviation (SD), with statistical analyses performed.

Statistical analysis. SPSS 21.0 (IBM, USA) was applied for data analysis. Measurement data were expressed as mean and SD from three independent tests. The comparison of normally distributed data between two groups was analyzed using an unpaired *t*-test. Data comparisons among multiple groups were performed using one-way analysis of variance (ANOVA) with a Tukey's post hoc test. Data comparison among groups at different timepoints was performed using repeated measures of ANOVA with Bonferroni's post hoc test. A p-value < 0.05 was considered to be reflective of statistical significance.

Results

miR-136-5p facilitates osteogenic differentiation in vivo and in vitro. In order to ascertain whether miR-136-5p plays a key role in the pathology of bone fracture and whether upregulation of miR-136-5p expression may promote fracture healing, we initially successfully surgically established a fracture mouse model, and subsequently conducted treatment with miR-136-5p overexpression oligonucleotides. RT-qPCR was subsequently performed to detect the expression of miR-136-5p in callus tissues, and the results indicated that relative to the sham group, the miR-136-5p expression was significantly reduced in the callus tissues of mice in the model group and model + agomir NC group ($p = 0.031$, one-way ANOVA). In addition, compared with the model + agomir NC group, the callus tissues of mice in the model + miR-136-5p group had elevated miR-1365p expression ($p = 0.014$, one-way ANOVA) (Figure 1a).

HE staining was applied to observe bone healing, with the results demonstrating normal TRAP and intact femoral staining in the sham group, while distinct fracture lines were identified in the model group and model + agomir NC group mice, with fibrous callus formation, discontinuous appearance of the cortical bone, ambiguous neonatal trabecular structure, as well as less new bone formation. Relative to the model + agomir NC group, the mice in the model + miR-136-5p group exhibited the diminished fracture ends, formation of fibrous callus, the increased neonatal trabecular structure, as well as an increase in new bone mass, indicative of superior fracture healing (Figure 1b). TRAP staining, which was used to calculate the number of positively stained osteoclasts, revealed that compared with the sham group, the number of TRAP positively stained osteoclasts was significantly reduced in the model group and model + agomir NC group ($p < 0.001$, one-way ANOVA). Meanwhile, compared with the model + agomir NC group, the number of TRAP-positive stained osteoclasts was markedly elevated in the model + miR-136-5p group ($p < 0.001$, one-way ANOVA) (Figures 1b and 1c). The ALP

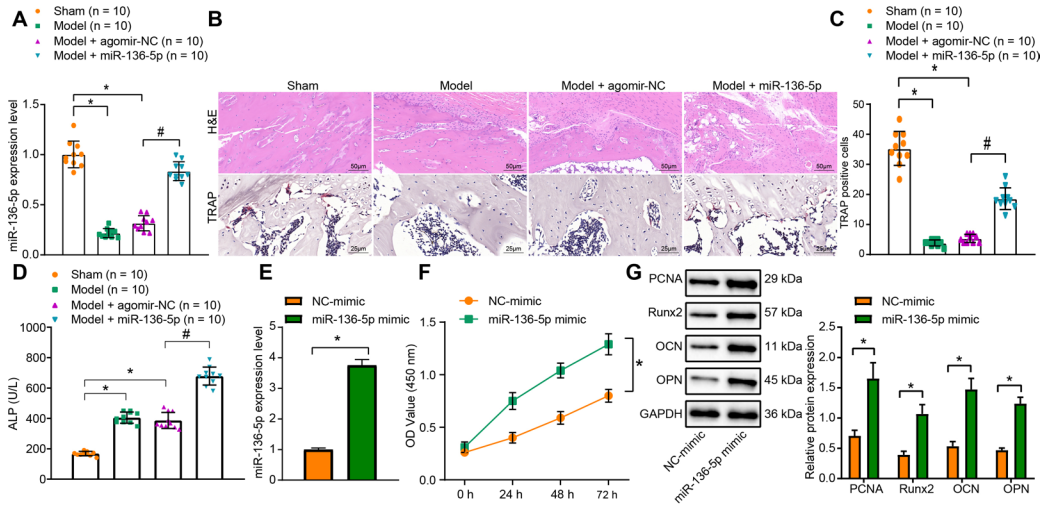

Fig. 1

miR-136-5p overexpression promotes osteogenic differentiation in vivo and in vitro. a) Reverse transcription quantitative polymerase chain reaction (RT-qPCR) detection of the expression of miR-136-5p in callus tissues of mice in each group; b) haematoxylin & eosin (HE) staining (× 200) and tartrate-resistant acid phosphatase (TRAP) staining (× 400) of bone healing situation of mice in each group; c) quantitative TRAP analysis of the number of positively stained osteoclasts in mice in each group; d) the disodium phenyl phosphate microplate method detection of the activity of alkaline phosphatase (ALP) in serum of mice in each group; e) RT-qPCR detection of the expression of microRNA (miR)-136-5p in MC3T3-E1 cells overexpressing miR-136-5p; f) Cell counting kit (CCK)-8 detection of the proliferation rate of MC3T3-E1 cells overexpressing miR-136-5p; g) Western blot detection of the protein expression of proliferating cell nuclear antigen (PCNA), Runt-related transcription factor 2 (Runx2), osteocalcin (OCN), osteopontin (OPN), and glyceraldehyde-3-phosphate dehydrogenase (GAPDH) in MC3T3-E1 cells overexpressing miR-136-5p. * indicates $p < 0.05$ compared with sham group or NC -mimic group and # indicates $p < 0.05$ compared with Model + agomir-NC. Measurement data were presented as mean and standard deviation. Unpaired *t*-test was used for data comparison between two groups. Data comparisons among multiple groups were performed using one-way analysis of variance (ANOVA) with Tukey's post hoc test. Data comparison among groups at different timepoints was performed by repeated measures ANOVA with Bonferroni's post hoc test. N = 10. The experiment was repeated three times.

activity in the serum was detected using the disodium phenyl phosphate microplate method, with the results suggesting that compared with the sham group, the ALP activity of the model and model + agomir NC groups was significantly increased ($p < 0.001$, one-way ANOVA). Meanwhile, the ALP activity was much higher in the model+ miR-136-5p group than the model + agomir NC group ($p < 0.001$, one-way ANOVA) (Figure 1d).

In an attempt to further elucidate the associated mechanism, osteoblast MC3T3-E1 cells were used to conduct the in vitro experiments. MC3T3-E1 cells were transfected with miR-136-5p mimic, after which RT-qPCR was performed to detect the expression of miR-136-5p. Evidence was obtained indicating that compared to the NC-mimic group, the expression of miR-136-5p in the miR-136-5p mimic group was significantly increased ($p < 0.001$, unpaired *t*-test) (Figure 1e).

In addition, CCK-8 assay was conducted to examine the proliferation ability of MC3T3-E1 cells in each group, the result of which indicated that compared with the NC-mimic group, the proliferation of MC3T3-E1 cells in the miR-136-5p mimic group was increased ($p < 0.001$, repeated measures of ANOVA) (Figure 1f). Finally, Western blot was performed to detect the expression of proteins related to cell proliferation (PCNA) and bone formation (Runx2, OCN, and OPN) in each group, with results illustrating that compared with the NC-mimic group, the protein expression of PCNA, Runx2, OCN, and OPN was increased significantly in the miR-136-5p mimic group ($p_{PCNA} = 0.004$, $p_{Runx2} = 0.002$, $p_{OCN} = 0.001$, $p_{OPN} < 0.001$, unpaired *t*-test) (Figure 1g).

Overall, the aforementioned results indicate that overexpression of miR-136-5p promotes the proliferation and differentiation of osteoblasts, thereby promoting fracture healing.

miR-136-5p is highly expressed in BMSCs and BMSC-derived exosomes. In view of the data suggesting that miR-13-5p was highly expressed in BMSC exosomes, BMSCs were cultured in vitro, and the growth morphology of BMSCs P4, as well as their osteogenic and adipogenic differentiation ability, were observed under an optical microscope. The results exhibited that BMSCs P4 cells were fusiform-like and grew in a parallel arrangement or in a swirl shape. The BMSCs were able to differentiate into osteoblasts under induction culture of the osteogenic differentiation; BMSCs are also capable of differentiating into adipocytes under induction culture of the adipogenic differentiation (Figure 2a). The BMSCs were confirmed to have been successfully cultured.

Furthermore, the exosomes derived from MLO-Y4 cells were regarded as the control for exosomes derived from BMSCs for subsequent experiments. Observation of the morphology of exosomes by transmission electron microscopy revealed that most of the exosomes were round or elliptical with varying sizes with a diameter of 30 nm to 150 nm (Figure 2b). Nanosight particle tracking analysis detected the size and number of exosomes, the result of which indicated that the collected exosomes

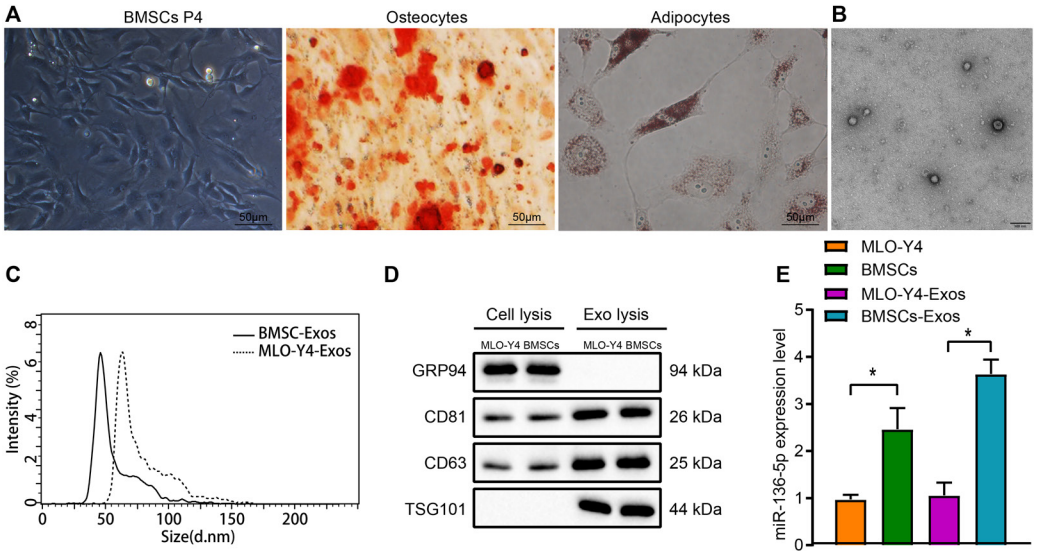

Fig. 2

miR-136-5p is highly expressed in bone marrow mesenchymal stem cells (BMSCs) and their exosomes. a) Morphological characteristics of BMSCs at passage 4 and alizarin red S and oil red O staining results of osteogenic as well as adipogenic differentiation observed under an optical microscope (× 200); b) exosome structure diagram observed under a transmission electron microscope after stained by phosphotungstic acid solution (scale bar = 100 nm); c) nanosight particle tracking analysis of the size and number of exosomes; d) Western blot detection of the protein expression of TSG101, CD63, CD81, and GRP94 in MLO-Y4, BMSCs, and their exosomes; e) reverse transcription quantitative polymerase chain reaction (RT-qPCR) detection of the expression of miR-136-5p in MLO-Y4, BMSCs and exosomes; * indicates $p < 0.05$. Measurement data were presented as mean and standard deviation. Unpaired *t*-test was used for data comparison between two groups. Data comparisons among multiple groups were performed using one-way analysis of variance (ANOVA) with Tukey's post hoc test. Data comparison among groups at different timepoints was performed by repeated measures ANOVA with Bonferroni's post hoc test. The experiment was repeated three times.

were generally distributed between 10 nm and 150 nm (Figure 2c). In addition, Western blot was performed to detect the expression of exosome-specific marker proteins (CD63, CD81, and TSG101) and endoplasmic reticulum markers (GRP94). It was found that compared with MLO-Y4 and BMSCs themselves, the expression of TSG101, CD63, and CD81 protein was significantly increased while GRP94 protein was scarcely expressed in MLO-Y4-Exos and BMSC-Exos ($p < 0.001$, one-way ANOVA) (Figure 2d).

Finally, RT-qPCR was performed to identify the expression of miR-136-5p in MLO-Y4, BMSCs, as well as their exosomes. The expression of miR-136-5p in BMSCs was higher than that of the MLO-Y4. In addition, compared with MLO-Y4-Exos, the expression of miR-136-5p in BMSC-Exos increased significantly ($p < 0.001$, one-way ANOVA) (Figure 2e). The aforementioned results demonstrated that miR-136-5p is highly expressed in BMSCs and their exosomes.

Delivery of miR-136-5p from BMSC-Exos to MC3T3-E1 promotes the proliferation and osteogenic differentiation of MC3T3-E1. In order to evaluate whether BMSC-Exos could enter MC3T3-E1, BMSC-Exos were labelled with PKH67 and added into MC3T3-E1 cell culture, and then the uptake of Exos by MC3T3-E1 was observed under the fluorescence microscope. The results exhibited no green fluorescence in the PBS + MC3T3-E1 group or the culture medium+ MC3T3-E1 group, while strong green fluorescence was detected in the cytoplasm of the BMSC-Exos + MC3T3-E1 group. In addition, the laser confocal microscope at greater magnification indicated that the uptake of BMSC-Exos had been successfully endocytosed by the MC3T3-E1 cells (Figure 3a). In addition, miR-136-5p in BMSC-Exos was labelled with Cy3, and then the uptake of Exos by MC3T3-E1 was observed under the fluorescence microscope via the content of Cy3-miR-136-5p in each group. No red fluorescence was found in the PBS + MC3T3-E1 group and culture medium + MC3T3-E1 group (no Cy3-miR-136-5p). Meanwhile, more than 60% of cells in the BMSC-Exos + MC3T3-E1 group exhibited red fluorescence (Cy3-miR-136-5p content is high) (Figure 3b), indicating that BMSC-Exos can carry miR-136-5p to MC3T3-E1 cells.

Furthermore, the expression of miR-136-5p in MC3T3-E1 cells in each group was detected by RT-qPCR. No significant difference in the miR-136-5p level was detected between the PBS + MC3T3-E1 group and the culture medium + MC3T3-E1 group. Compared with the culture medium + MC3T3-E1 group, the expression of miR-136-5p in the BMSC-Exos + MC3T3-E1 group was significantly increased ($p = 0.002$, one-way ANOVA) (Figure 3c). In addition, the results of CCK-8 assay revealed there to be no significant difference in relation to the proliferation ability of the MC3T3-E1 cells between the PBS + MC3T3-E1 group and the culture medium + MC3T3-E1 group. Yet, compared with the culture medium + MC3T3-E1 group, the proliferation rate of MC3T3-E1 cells was increased in the BMSC-Exos + MC3T3-E1 group ($p < 0.001$, one-way ANOVA) (Figure 3d). The expression of proliferation related proteins (PCNA) and bone

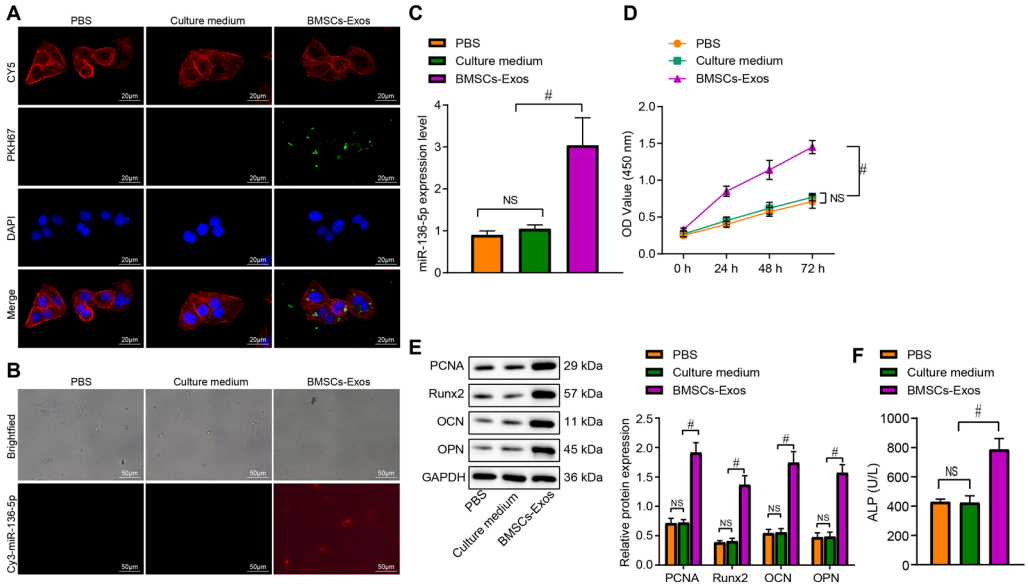

Fig. 3

miR-136-5p-containing bone marrow mesenchymal stem cell (BMSC)-Exos translocate to MC3T3-E1 and promote its proliferation and osteogenic differentiation. a) BMSC-Exos were labelled with PKH67, and the uptake of BMSC-Exos by MC3T3-E1 was observed under a fluorescence microscope (× 500). The Diluent C labelled cell membrane exhibit red fluorescence, the nuclei exhibit blue fluorescence, and PKH67 labelled Exos exhibit green fluorescence; b) fluorescence microscope observation of the content of Cy3 labelled miR-136-5p in BMSC-Exos in each treatment group with Cy3 exhibiting red fluorescence (× 200); c) reverse transcription quantitative polymerase chain reaction (RT-qPCR) detection of the expression of miR-136-5p in MC3T3-E1 cells treated with BMSC-Exos; d) cell counting kit (CCK)-8 detection of the proliferation rate of MC3T3-E1 cells treated with BMSC-Exos; e) Western blot detection of the protein expression of proliferating cell nuclear antigen (PCNA), Runt-related transcription factor 2 (Runx2), osteocalcin (OCN), osteopontin (OPN), and glyceraldehyde-3-phosphate dehydrogenase (GAPDH) in MC3T3-E1 cells treated with BMSC-Exos; f) alkaline phosphatase (ALP) activity in supernatant of MC3T3-E1 cells treated with BMSC-Exos detected by disodium phosphate microplate method; # indicates $p < 0.05$, and non-significant (NS) represents $p > 0.05$. Measurement data were presented as mean and standard deviation. Unpaired *t*-test was used for data comparison between two groups. Data comparisons among multiple groups were performed using one-way analysis of variance (ANOVA) with Tukey's post hoc test. Data comparison among groups at different timepoints was performed by repeated measures ANOVA with Bonferroni's post hoc test. The experiment was repeated three times. NS, non-significant; PBS, phosphate-buffered saline.

formation-related proteins (Runx2, OCN, and OPN) in MC3T3-E1 cells in each group was detected by Western blot, which failed to exhibit any notable difference in terms of the expression of PCNA, Runx2, OCN, and OPN between the PBS + MC3T3-E1 group and the culture medium + MC3T3-E1 group. However, when compared to the culture medium + MC3T3-E1 group, the expression of PCNA, Runx2, OCN, and OPN was upregulated in the BMSC-Exos + MC3T3-E1 group ($p_{PCNA} < 0.001$, $p_{Runx2} < 0.001$, $p_{OCN} < 0.001$, $p_{OPN} < 0.001$, one-way ANOVA) (Figure 3e). Besides, the activity of ALP in cell supernatant detected by disodium phenyl phosphate microplate method displayed no notable difference between the PBS + MC3T3-E1 group and the culture medium+ MC3T3-E1 group. Consistent with the findings of the other assays, relative to the culture medium + MC3T3-E1 group, the ALP activity was enhanced in the BMSC-Exos + MC3T3-E1 group ($p < 0.001$, one-way ANOVA) (Figure 3f). Collectively, the above results demonstrated that BMSC-Exos could translocate miR-136-5p to MC3T3-E1, thus promoting MC3T3-E1 proliferation and osteogenic differentiation.

miR-136-5p inhibits LRP4 expression to activate the Wnt/β-catenin pathway. The downstream target genes of miR-136-5p were predicted in connection with the TargetScan website, which revealed the presence of miR-136-5p binding sites in the 3'-UTR of LRP4 mRNA (Figure 4a). In addition, LRP4 has been documented to inhibit bone formation and the proliferation as well as differentiation of bone cells.[24] Therefore, we suspected that miR-136-5p can inhibit LRP4 expression. Dual luciferase reporter gene assay was subsequently performed to verify the predicted targeting between miR-136-5p and LRP4. Compared with the NC-mimic group, the luciferase signal of LRP4-WT was markedly diminished in the miR-136-5p mimic group ($p < 0.001$, unpaired *t*-test), while that of LRP4-MUT had no changes ($p = 0.852$, unpaired *t*-test) (Figure 4a), indicating that miR-136-5p can specifically bind to the LRP4 3'-UTR.

Furthermore, the relationship between miR-136-5p and LRP4 was investigated in MC3T3-E1 cells. Firstly, MC3T3-E1 cells were transfected with miR-136-5p mimic or inhibitor with their transfection efficiency evaluated by RT-qPCR. The results obtained provided verification confirming that miR-136-5p mimic and miR-136-5p inhibitor had indeed been successfully expressed in the cells ($p < 0.001$, unpaired *t*-test) (Figures 4b and 4c). Additionally, Western blot analysis illustrated that the overexpression of miR-136-5p inhibited the protein expression of LRP4 while silencing of miR-136-5p promoted the expression

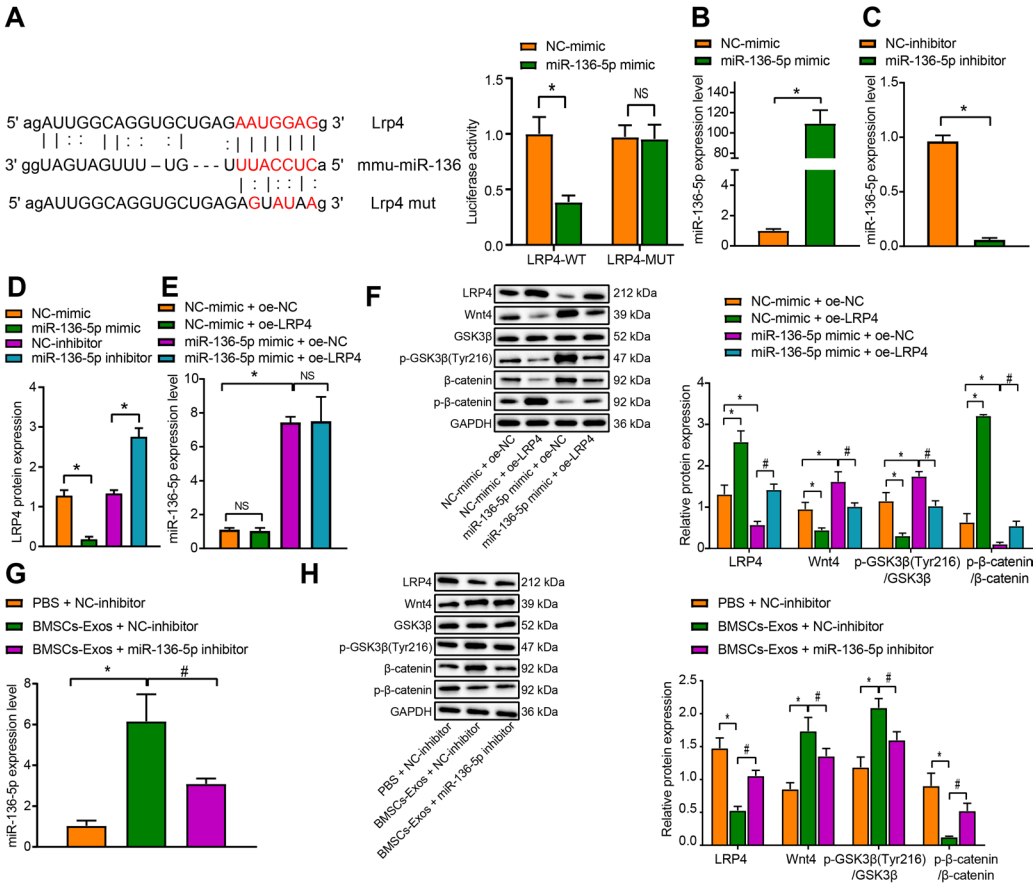

Fig. 4

MicroRNA (miR)-136-5p activates the Wnt/β-catenin pathway by targeting low-density lipoprotein receptor related protein 4 (LRP4). a) miR-136-5p binding sites in the LRP4 3'-untranslated region (3'-UTR) predicted by the TargetScan website, and binding of miR-136-5p to LRP4 confirmed by dual luciferase reporter gene assay in HEK293 cells; b) reverse transcription quantitative polymerase chain reaction (RT-qPCR) detection of the transfection efficiency of miR-136-5p mimic in MC3T3-E1 cells; c) RT-qPCR detection of the transfection efficiency of miR-136-5p inhibitor in MC3T3-E1 cells; d) Western blot detection of the protein expression of LRP4 in MC3T3-E1 cells with miR-136-5p overexpression or silencing; e) RT-qPCR detection of the expression of miR-136-5p in MC3T3-E1 cells transfected with miR-136-5p mimic, oe-LRP4, or both; f) Western blot detection of the expression of LRP4 and Wnt/β-catenin pathway related proteins in MC3T3-E1 cells transfected with miR-136-5p mimic, oe-LRP4, or both; g) RT-qPCR detected the expression of miR-136-5p in MC3T3-E1 cells treated with BMSC-Exos or in combination with miR-136-5p inhibitor; h) Western blot detection of the expression of LRP4 and Wnt/β-catenin pathway related proteins in MC3T3-E1 cells treated with BMSC-Exos or in combination with miR-136-5p inhibitor. # indicates $p < 0.05$, and non-significant (NS) represents $p > 0.05$. Measurement data were presented as mean and standard deviation. Unpaired *t*-test was used for data comparison between two groups while data comparisons among multiple groups were performed using one-way analysis of variance (ANOVA) with Tukey's post hoc test. Data comparison among groups at different timepoints was performed by repeated measurement ANOVA with Bonferroni's post hoc test. The experiment was repeated three times. MUT, mutant; PBS, phosphate-buffered saline; WT, wild type.

of LRP4 ($p < 0.001$, one-way ANOVA) (Figure 4d). Taken together, the above results suggested that miR-136-5p could target LRP4 and inhibit its expression.

LRP4 has been previously suggested to negatively regulate the Wnt/β-catenin pathway.[17] Consistent with previous results indicating the ability of miR-136-5p to inhibit the expression of LRP4, we set out to subsequently determine whether miR-136-5p could activate the Wnt/β-catenin pathway by targeting LRP4. Overexpression of miR-136-5p and upregulation of LRP4 were conducted on MC3T3-E1 cells, and then RT-qPCR as well as Western blot was used to detect the expression of miR-136-5p, LRP4, and Wnt/β-catenin pathway-related proteins. Compared with the NC-mimic + oe NC group, no difference in the miR-136-5p expression was found in the NC-mimic + oe-LRP4 group, while the expression of Wnt4, pGSK3β (Tyr216), and β-catenin was decreased significantly ($p_{LRP4} = 0.001$, $p_{p\text{-}\beta\text{-catenin}} < 0.001$, $p_{Wnt4} = 0.016$, $p_{p\text{-GSK3}\beta\ (Tyr216)} < 0.001$, $p_{\beta\text{-catenin}} < 0.001$, one-way ANOVA). However, besides miR-136-5p, expression of Wnt4, pGSK3β (Tyr216), and β-catenin was increased significantly in miR-136-5p mimic + oe NC group with notably decreased LRP4 expression and β-catenin phosphorylation extent ($p_{miR\text{-}136\text{-}5p} < 0.001$, $p_{LRP4} = 0.007$, $p_{p\text{-}\beta\text{-catenin}} = 0.009$, $p_{Wnt4} = 0.003$, $p_{p\text{-GSK3}\beta\ (Tyr216)} = 0.001$, $p_{\beta\text{-catenin}} < 0.001$, one-way ANOVA). Compared with the miR-136-5p mimic + oe NC group, miR-136-5p expression did not exhibit any distinct changes in the miR-136-5p mimic + oe-LRP4 group, while LRP4 level and β-catenin phosphorylation extent were increased significantly with decreased Wnt4, pGSK3β (Tyr216), and β-catenin expression ($p_{LRP4} = 0.003$, $p_{p\text{-}\beta\text{-catenin}} = 0.013$, $p_{Wnt4} = 0.006$, p

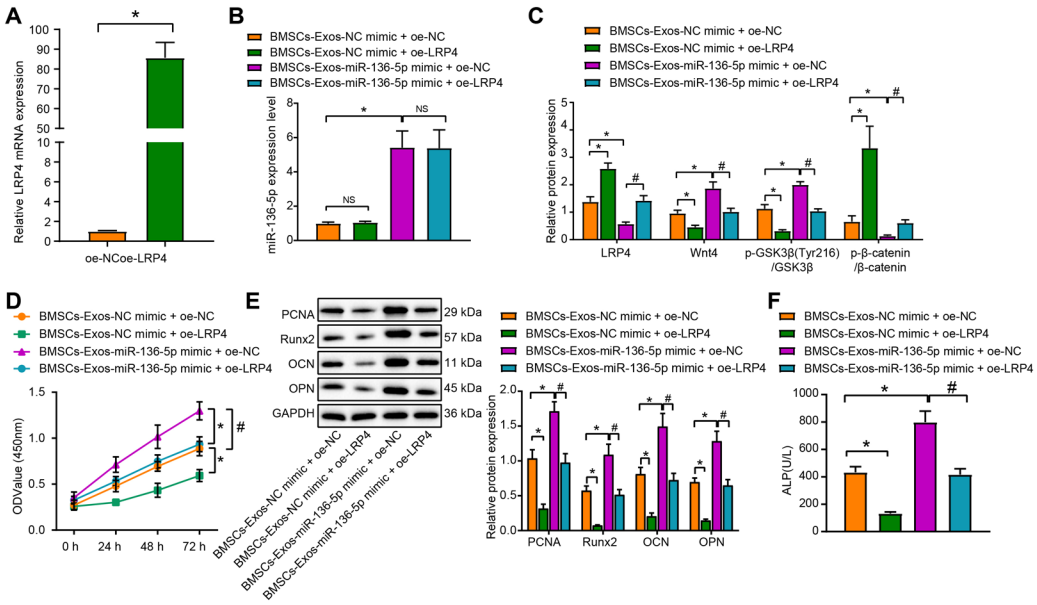

Fig. 5

miR-136-5p-containing bone marrow mesenchymal stem cell (BMSC)-Exos regulate low-density lipoprotein receptor related protein 4 (LRP4)/Wnt/β-catenin axis to promote MC3T3-E1 proliferation and osteogenic differentiation. a) Reverse transcription quantitative polymerase chain reaction (RT-qPCR) detection of the transfection efficiency of LRP4 overexpression in MC3T3-E1 cells; MC3T3-E1 cells were treated with exosomes from miR-136-5p mimic-transfected BMSCs, or in combination with oe-LRP4. b) RT-qPCR detection of the expression of miR-136-5p in MC3T3-E1 cells; c) Western blot detection of the expression of LRP4 and Wnt/β-catenin pathway related proteins in MC3T3-E1 cells; d) cell counting kit (CCK)-8 detection of the proliferation rate of MC3T3-E1 cells; e) Western blot detection of the protein expression of proliferating cell nuclear antigen (PCNA), Runt-related transcription factor 2 (Runx2), osteocalcin (OCN), and osteopontin (OPN) in MC3T3-E1 cells; f) alkaline phosphatase (ALP) activity of the supernatant of MC3T3-E1 cells detected by disodium phenyl phosphate microplate method. * and # indicate $p < 0.05$, and NS represents $p > 0.05$. Measurement data were presented as mean and standard deviation. Unpaired *t*-test was used for data comparison between two groups. Data comparisons among multiple groups were performed using one-way analysis of variance (ANOVA) with Tukey's post hoc test. Data comparison among groups at different timepoints was performed by repeated measures ANOVA with Bonferroni's post hoc test. The experiment was repeated three times. mRNA, messenger RNA; NS, non-significant.

$p_{p\text{-GSK3β (Tyr216)}} < 0.001$, $p_{β\text{-catenin}} < 0.001$, one-way ANOVA) (Figures 4e and 4f).

Finally, the MC3T3-E1 cells were treated with PBS, NC-inhibitor, BMSC-Exos, and miR-136-5p inhibitor, respectively. The results of RT-qPCR and Western blot demonstrated that relative to the PBS + NC-inhibitor group, the expression of miR-136-5p, Wnt4, and β-catenin along with GSK3β (Tyr216) phosphorylation extent was increased, while that of LRP4 and β-catenin phosphorylation extent were decreased significantly in the BMSC-Exos + NC-inhibitor group ($p_{miR\text{-}136\text{-}5p} < 0.001$, $p_{LRP4} < 0.001$, $p_{p\text{-}β\text{-}catenin} < 0.001$, $p_{Wnt4} < 0.001$, $p_{p\text{-GSK3β (Tyr216)}} = 0.036$, $p_{β\text{-}catenin} = 0.013$, one-way ANOVA). Meanwhile, the expression of miR-136-5p, Wnt4, and β-catenin along with GSK3β (Tyr216) phosphorylation extent in the BMSC-Exos + miR-136-5p inhibitor group was significantly lower than that of the BMSC-Exos + NC-inhibitor group; however, LRP4 expression and β-catenin phosphorylation extent were increased significantly ($p_{miR\text{-}136\text{-}5p} = 0.008$, $p_{LRP4} = 0.002$, $p_{p\text{-}β\text{-}catenin} = 0.009$, $p_{Wnt4} = 0.045$, $p_{p\text{-GSK3β (Tyr216)}} = 0.037$, $p_{β\text{-}catenin} = 0.043$, one-way ANOVA) (Figures 4g and 4h). There was no statistically significant difference in the expression of GSK3β among all the groups. The above results demonstrate that miR-136-5p activates the Wnt/β-catenin pathway by inhibiting LRP4 expression, and furthermore, miR-136-5p-containing BMSC-Exos also play a similar role in activating the Wnt/β-catenin pathway by inhibiting LRP4 expression.

BMSC-Exos-carried miR-136-5p targets LRP4/Wnt/β-catenin axis to promote the proliferation and osteogenic differentiation of MC3T3-E1. Since BMSC-Exos-carried miR-136-5p was found to regulate the LRP4/Wnt/β-catenin pathway, we subsequently investigated whether miR-136-5p-containing BMSC-Exos could promote the proliferation and osteogenic differentiation of MC3T3-E1 by targeting the LRP4/Wnt/β-catenin axis. The RT-qPCR results confirmed successful transfection of LRP4 overexpression in MC3T3-E1 cells ($p < 0.001$, unpaired *t*-test) (Figure 5a). Moreover, MC3T3-E1 cells were treated with BMSC-Exos-NC mimic, BMSC-Exos-miR-136-5p mimic, oe-NC, and oe-LRP4, respectively. RT-qPCR data revealed that compared with the BMSC-Exos-NC mimic + oe NC group, no distinct difference in terms of miR-136-5p expression was identified in the BMSC-Exos-NC mimic + oe-LRP4 group while the expression of LRP4 and β-catenin phosphorylation extent were significantly increased, along with decreased expression of Wnt4, and β-catenin along with GSK3β (Tyr216) phosphorylation extent ($p_{LRP4} = 0.001$, $p_{p\text{-}β\text{-}catenin} < 0.001$, $p_{Wnt4} = 0.015$, $p_{p\text{-GSK3β (Tyr216)}} < 0.001$, $p_{β\text{-}catenin} = 0.027$, one-way ANOVA). However, the expression of miR-136-5p, Wnt4, and β-catenin along with GSK3β

(Tyr216) phosphorylation extent was all markedly increased, with the expression of LRP4 and β-catenin phosphorylation extent significantly reduced in the BMSC-Exos-miR-136-5p mimic + oe NC group, compared with BMSC-Exos-NC mimic + oe NC group (p_{LRP4} = 0.002, $p_{p\text{-}\beta\text{-}catenin}$ < 0.001, p_{Wnt4} < 0.001, $p_{p\text{-}GSK3\beta\ (Tyr216)}$ < 0.001, $p_{\beta\text{-}catenin}$ = 0.002, one-way ANOVA). In comparison with the BMSC-Exos-miR-136-5p mimic + oe NC group, the BMSC-Exos-miR-136-5p mimic + oe-LRP4 group showed no changes in the expression of miR-136-5p, increased LRP4 expression and β-catenin phosphorylation extent, and decreased Wnt4 and β-catenin expression along with GSK3β (Tyr216) phosphorylation extent (p_{LRP4} = 0.001, $p_{p\text{-}\beta\text{-}catenin}$ < 0.001, p_{Wnt4} < 0.001, $p_{p\text{-}GSK3\beta\ (Tyr216)}$ < 0.001, $p_{\beta\text{-}catenin}$ = 0.003, one-way ANOVA) (Figures 5b and 5c).

In addition, CCK-8 assay revealed that relative to the BMSC-Exos-NC mimic + oe NC group, the proliferation of MC3T3-E1 cells in the BMSC-Exos-NC mimic + oe-LRP4 group was inhibited, while an opposite trend was observed in the miR-136-5p mimic + oe NC group (p < 0.05). Treatment with BMSC-Exos-miR-136-5p mimic and overexpression of LRP4 could inhibit the proliferation of MC3T3-E1 cells (p < 0.001, repeated measures of ANOVA) (Figure 5d). Moreover, the protein expression of PCNA, Runx2, OCN, and OPN in the BMSC-Exos-NC mimic + oe-LRP4 group was significantly decreased (p_{PCNA} < 0.001, p_{Runx2} < 0.001, p_{OCN} = 0.001, p_{OPN} < 0.001, one-way ANOVA) when compared to the BMSC-Exos-NC mimic + oe NC group, while a contrasting result was obtained in relation to the BMSC-Exos-miR-136-5p mimic + oe-LRP4 group relative to the BMSC-Exos-miR-136-5p mimic + oe NC group (p_{PCNA} < 0.001, p_{Runx2} < 0.001, p_{OCN} < 0.001, p_{OPN} < 0.001, one-way ANOVA) (Figure 5e).

Compared with the BMSC-Exos-NC mimic + oe NC group, ALP activity was significantly decreased in the BMSC-Exos-NC mimic + oe-LRP4 group, while it was significantly increased in the BMSC-Exos-miR-136-5p mimic + oe NC group (p < 0.001, one-way ANOVA). Additionally, in comparison to the BMSC-Exos-miR-136-5p mimic + oe NC group, the ALP activity was significantly decreased in BMSC-Exos-miR 136-5p mimic + oe-LRP4 group (p < 0.001, one-way ANOVA) (Figure 5f). No statistically significant difference was detected in regard to the expression of GSK3β among all the groups. The aforementioned results indicate that BMSC-Exos-carried miR-136-5p can target and regulate the LRP4/Wnt/β-catenin axis to promote the proliferation and osteogenic differentiation of MC3T3-E1 cells.

BMSC-Exos-carried miR-136-5p targets LRP4 and activates the Wnt/β-catenin pathway to promote fracture healing. The effect of miR-136-5p-containing BMSC-Exos on regulation of LRP4/Wnt/β-catenin axis, and additionally on the fracture healing, was subsequently investigated in vivo. The MC3T3-E1 cells were transfected with DKK1 overexpression plasmids with RT-qPCR employed to verify whether DKK1 could be successfully overexpressed in MC3T3-E1 cells (p < 0.001, unpaired *t*-test) (Figure 6a). Subsequent results from RT-qPCR and Western blot demonstrated that compared to the model + NC-mimic-Exos + oe NC group, Wnt4 and β-catenin expression along with GSK3β (Tyr216) phosphorylation extent was diminished significantly in the model + NC-mimic-Exos + oe-DKK1 group, whereas β-catenin phosphorylation extent was augmented (p < 0.001, one-way ANOVA). However, no significant difference in terms of the expression of miR-136-5p was detected between these two groups. Meanwhile, the expression of miR-136-5p, Wnt4, and β-catenin along with GSK3β (Tyr216) phosphorylation extent was increased significantly, while the expression of LRP4 and β-catenin phosphorylation extent was significantly decreased in the model + miR-136-5p mimic-Exos + oe NC group when compared with the model + NC-mimic-Exos + oe NC group (p < 0.001, one-way ANOVA). In addition, the expression of Wnt4, pGSK3β (Tyr216), and β-catenin was significantly reduced, and the β-catenin phosphorylation extent was elevated (p < 0.001, one-way ANOVA) in the model + miR-136-5p mimic-Exos + oe-DKK1 group with no significant difference observed in terms of the expression of miR-136-5p and LRP4, compared with the model + miR-136-5p mimic-Exos + oe NC group (Figures 6b and 6c). There was no statistically significant difference in terms of the expression of GSK3β among all the groups.

Moreover, immunohistochemical detection of β-catenin positive expression found that compared with the model+ NC-mimic-Exos + oe NC group, the positive expression rate of β-catenin protein was reduced in the model + NC-mimic-Exos + oe-DKK1 group, which was reversed in the model + miR-136-5p mimic-Exos + oe NC group (p < 0.001, one-way ANOVA). Meanwhile, the β-catenin protein positive rate was significantly decreased (p < 0.001, one-way ANOVA) in the model + miR-136-5p mimic-Exos + oe-DKK1 group, compared with the model + miR-136-5p mimic-Exos + oe NC group (Figure 6d). Analysis of HE staining on bone healing suggested that compared with the model + NC-mimic-Exos + oe NC group, fracture healing was notably slowed in the model + NC-mimic-Exos + oe-DKK1 group, but it was better in the model + miR-136-5p mimic-Exos + oe NC group. Meanwhile, compared with the model+ miR-136-5p mimic-Exos + oe NC group, the model + miR-136-5p mimic-Exos + oe-DKK1 group exhibited a slower rate of fracture healing (p < 0.001, one-way ANOVA) (Figure 6e). Further, TRAP staining revealed a smaller number of TRAP positively stained osteoclasts in the model + NC-mimic-Exos + oe-DKK1 group, while a greater number was detected in the model + miR-136-5p mimic-Exos + oe NC group than the model + NC-mimic-Exos + oe NC group (p < 0.001, one-way ANOVA). Meanwhile, compared with the model + miR-136-5p mimic-Exos + oe NC group, the number of TRAP positively stained osteoclasts was decreased in the model + miR-136-5p mimic-Exos + oe-DKK1 group (p < 0.001, one-way ANOVA) (Figure 6f).

Western blot further demonstrated that in the fracture tissues of mice in the model + NC-mimic-Exos +

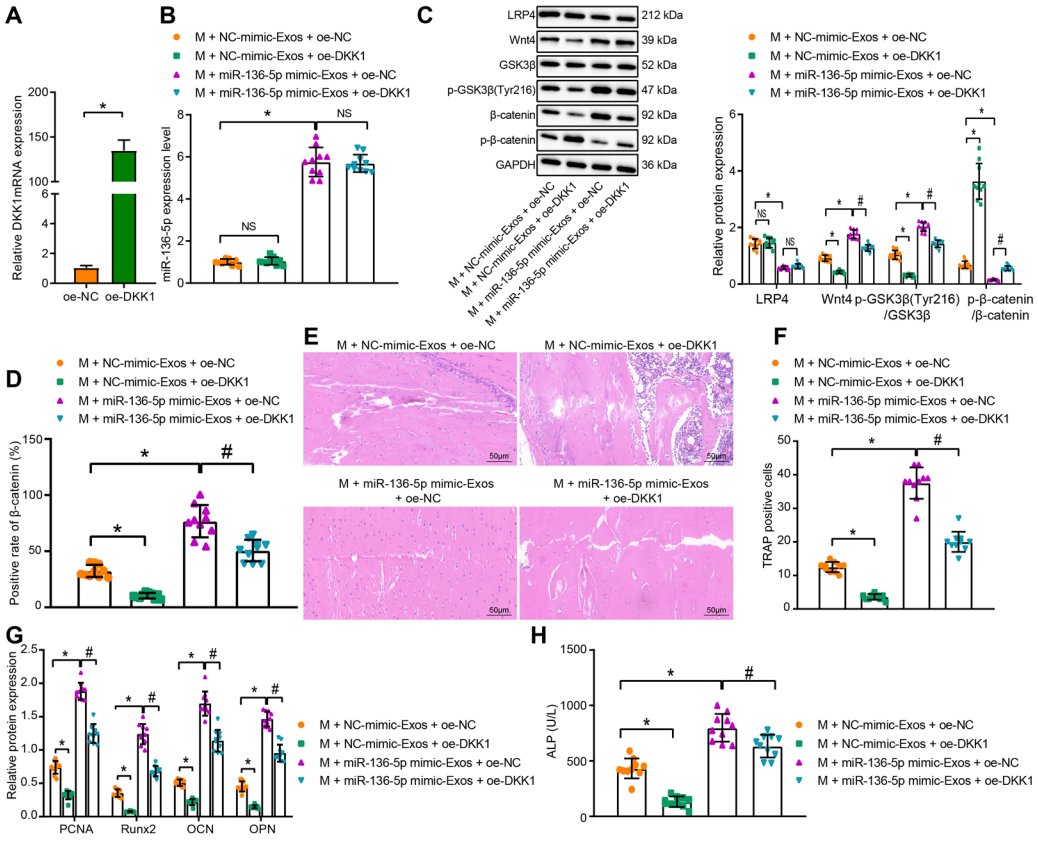

Fig. 6

Bone marrow mesenchymal stem cell (BMSC)-Exos-carried miR-136-5p inhibits LRP4 expression and activates the Wnt/β-catenin pathway to facilitate fracture healing. a) Reverse transcription quantitative polymerase chain reaction (RT-qPCR) detection of the transfection efficiency of DKK1 overexpression in MC3T3-E1 cells; mice were treated with oe-DKK1, exosomes from miR-136-5p mimic-transfected BMSCs, or both. b) RT-qPCR detection of the expression of miR-136-5p in mouse fracture tissues; c) Western blot detection of the expression of LRP4 and Wnt/β-catenin pathway related proteins in the mouse fracture tissues; d) immunohistochemistry analysis of β-catenin protein in the mouse fracture tissues; e) haematoxylin and eosin staining of the bone healing degree in mouse fracture tissues (× 200); f) tartrate-resistant acid phosphatase (TRAP) staining analysis of positively stained osteoclasts in mouse fracture tissues; g) Western blot detection of the protein expression of proliferating cell nuclear antigen (PCNA), Runt-related transcription factor 2 (Runx2), osteocalcin (OCN), and osteopontin (OPN) in the mouse fracture tissues; h) alkaline phosphatase (ALP) activity in the serum of mice detected by disodium phenyl phosphate microplate method. * and # indicate $p < 0.05$, and NS represents $p > 0.05$. Measurement data were presented as mean and standard deviation. Unpaired *t*-test was used for data comparison between two groups. Data comparisons among multiple groups were performed using one-way analysis of variance (ANOVA) with Tukey's post hoc test. Data comparison among groups at different timepoints was performed by repeated measures ANOVA with Bonferroni's post hoc test. N = 10. The experiment was repeated three times. mRNA, messenger RNA; NS, non-significant.

oe-DKK1 group, the expression of PCNA, Runx2, OCN, and OPN was downregulated but an opposite result was yielded in the model + miR-136-5p mimic-Exos + oe NC group as compared with the model + NC-mimic-Exos + oe NC group ($p < 0.001$, one-way ANOVA). In addition, when compared to the model + miR-136-5p mimic-Exos + oe NC group, a decline was noted in the expression of PCNA, Runx2, OCN, and OPN in the model + miR-136-5p mimic-Exos + oe-DKK1 group ($p < 0.001$, one-way ANOVA) (Figure 6g). Furthermore, compared with the model + NC-mimic-Exos + oe NC group, the ALP activity was significantly decreased in the model + NC-mimic-Exos + oe-DKK1 group while it was significantly increased in the model+ miR-136-5p mimic-Exos + oe NC group ($p < 0.001$, one-way ANOVA). In addition, the ALP activity was markedly lower in the model + miR-136-5p mimic-Exos + oe-DKK1 group than in the model + miR-136-5p mimic-Exos + oe NC group ($p < 0.001$, one-way ANOVA) (Figure 6h). All the above results indicated that miR-136-5p-containing BMSC-Exos inhibited the expression of LRP4 and activated the Wnt/β-catenin pathway to promote fracture healing (Figure 7).

Discussion

The osteogenic differentiation of human BMSCs is a central issue in fracture healing, with miRNAs recently emerging as crucial participants in this process.[25,26] During the current study, we set out to explore the mechanism by which exosomes derived from mouse BMSCs carry miR-136-5p in relation to fracture healing. The key findings indicated that miR-136-5p shuttled by BMSC-derived exosomes had the potential to inhibit the expression of LRP4 gene and subsequently activated the Wnt/β-catenin pathway, hence potentiating osteogenic proliferation and differentiation, which ultimately facilitated the fracture healing process.

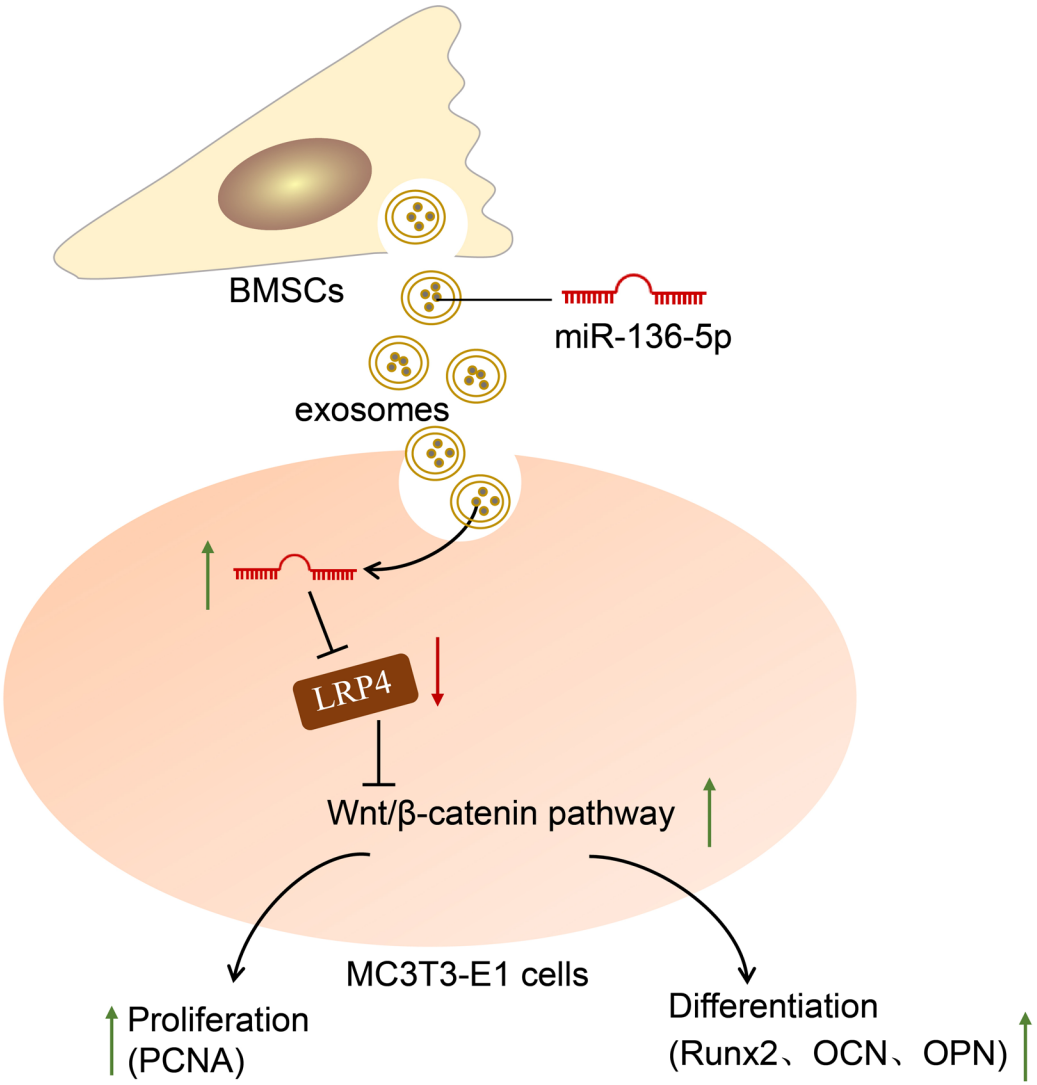

Fig. 7

Mechanical graph of microRNA (miR)-136-5p from bone marrow mesenchymal stem cell (BMSC)-derived exosomes facilitates fracture healing by targeting LRP4 to activate the Wnt/β-catenin pathway. LRP4, low-density lipoprotein receptor related protein 4; OCN, osteocalcin; OPN, osteopontin; PCNA, proliferating cell nuclear antigen; Runx2, Runt-related transcription factor 2.

miR-136-5p was initially identified to promote osteogenic proliferation and differentiation in vivo and in vitro, which was manifested by an increased expression of PCNA, Runx2, OCN, and OPN proteins. Runx2 is known to be required for the proliferation of osteoblast progenitors.[27] OPN has been demonstrated in a previous study to regulate the cell proliferation of certain types of cancer cells, while other literature has highlighted its involvement in wound healing as well as bone remodelling.[28–30] OCN represents an osteogenic marker protein[31] with its expression, when upregulated, shown to be a useful aid in relation to the promotion of osteoblast differentiation.[32] As a proliferation marker, PCNA and its elevated expression has been highlighted as a hallmark of accelerated proliferation of osteoblasts in osteoporosis rats.[33] The aforementioned evidence highlights the capability of miR-136-5p to promote osteogenic proliferation and differentiation. In addition, a previous study concluded that miR-136-3p could target phosphatase and tensin homolog deleted on chromosome ten (PTEN) in both human umbilical vein endothelial cells (HUVECs) and BMSCs, thus substantially enhancing vascularization and osteogenic differentiation and ameliorating alcohol-induced osteopenia.[34] A key observation made during our study suggested that miR-136-5p-containing exosome treatment induced the activation of osteoclastogenesis during bone fracture healing. In view of the homology of miR-136-3p and miR-136-5p, we suspected that miR-136-5p may also play a key role similar to that of miR-136-3p in the regulation of vascularization as well as bone formation.

Moreover, our data indicated that the overexpression of miR-136-5p occurred in BMSCs and BMSC-derived

exosomes. Consistent with our finding, previous literature has also demonstrated that miR-136-5p is expressed at high levels in exosomes derived from BMSCs.[20] Additionally, a notable finding of the present study revealed that BMSC-derived exosomes could deliver miR-136-5p to MC3T3-E1 cells and subsequently promotes the proliferation and differentiation of MC3T3-E1 cells. BMSCs can package miRNAs into exosomes, and these engineered exosomes can systemically deliver these miRNAs to recipient cells.[35] Consistent with our data, exosomes derived from BMSCs have been reported to possess the capacity to enhance osteogenic proliferation and differentiation in vitro, as well as markedly accelerating bone regeneration during distraction osteogenesis in older rats.[36] BMSC-derived exosomal miR-136-5p was found to promote chondrocyte migration in vitro and reduce cartilage degeneration in vivo, thus inhibiting osteoarthritis pathology.[37] Therefore, miR-136-5p delivered by BMSC-derived exosomes may play an integral role during bone fracture repair, and represents a promising therapeutic target to improve the fracture healing process.

Furthermore, we substantiated that LRP4 is targeted and reversely regulated by miR-136-5p. Previous research has suggested that miRNAs may modulate gene expression post-transcriptionally by interacting with the 3′-UTR of specific target mRNAs, resulting in the inhibition of mRNA degradation or translation.[38] LRP4 has been confirmed to be a target gene of another miRNA, miR-490-3p, in skeletal muscle cells.[39]

Another key observation made during the current study indicated that miR-136-5p inhibited LRP4 expression to activate the Wnt/β-catenin pathway. LRP4 has been reported to be a susceptibility genetic locus for osteoporotic fracture in postmenopausal Chinese women.[40] The ability of LRP4 to exert suppressive effects on bone formation and proliferation, as well as differentiation of bone cells, has been emphasized in previous work.[30] Moreover, LRP4 negatively regulates the Wnt/β-catenin pathway during osteoblastic differentiation.[41] Accumulating evidence continues to demonstrate that the Wnt/β-catenin pathway can promote the proliferation and differentiation of bone cells, and bone formation, thereby facilitating fracture healing.[21,42] Thus, we reasoned that exosome-encapsulated miR-136-5p from BMSCs may promote the osteogenic proliferation and differentiation by targeting the LRP4/Wnt/β-catenin signalling axis.

Taken together, the current study presents evidence demonstrating that miR-136-5p delivered via exosomes from BMSCs may potentially promote fracture healing, whereby miR-136-5p activates the Wnt/β-catenin pathway via LRP4 inhibition, and consequently enhances osteogenic proliferation and differentiation. This paracrine transfer of miRs may represent a new approach towards miR-based therapy in fracture healing.

Supplementary material

Table of primer sequences for reverse transcription quantitative polymerase chain reaction and ARRIVE checklist.

References

1. **Jiang B**, **Liang S**, **Peng ZR**, **et al**. Transport and public health in China: the road to a healthy future. *Lancet*. 2017;390(10104):1781–1791.
2. **Grzonka P**, **Rybitschka A**, **De Marchis GM**, **Marsch S**, **Sutter R**. Bone fractures from generalized convulsive seizures and status epilepticus-A systematic review. *Epilepsia*. 2019;60(5):996–1004.
3. **Marsell R**, **Einhorn TA**. The biology of fracture healing. *Injury*. 2011;42(6):551–555.
4. **Komatsu DE**, **Warden SJ**. The control of fracture healing and its therapeutic targeting: improving upon nature. *J Cell Biochem*. 2010;109(2):302–311.
5. **Trajkovic K**, **Hsu C**, **Chiantia S**, **et al**. Ceramide triggers budding of exosome vesicles into multivesicular endosomes. *Science*. 2008;319(5867):1244–1247.
6. **Trams EG**, **Lauter CJ**, **Salem N**, **Heine U**. Exfoliation of membrane ecto-enzymes in the form of micro-vesicles. *Biochim Biophys Acta*. 1981;645(1):63–70.
7. **Morelli AE**, **Larregina AT**, **Shufesky WJ**, **et al**. Endocytosis, intracellular sorting, and processing of exosomes by dendritic cells. *Blood*. 2004;104(10):3257–3266.
8. **Zhang S**, **Chu WC**, **Lai RC**, **Lim SK**, **Hui JH**, **Toh WS**. Exosomes derived from human embryonic mesenchymal stem cells promote osteochondral regeneration. *Osteoarthritis Cartilage*. 2016;24(12):2135–2140.
9. **Heldring N**, **Mager I**, **Wood MJ**, **Le Blanc K**, **Andaloussi SE**. Therapeutic potential of multipotent mesenchymal stromal cells and their extracellular vesicles. *Hum Gene Ther*. 2015;26(8):506–517.
10. **Ambros V**. The functions of animal microRNAs. *Nature*. 2004;431(7006):350–355.
11. **Takahara S**, **Lee SY**, **Iwakura T**, **et al**. Altered expression of microRNA during fracture healing in diabetic rats. *Bone Joint Res*. 2018;7(2):139–147.
12. **Bartel DP**. Micrornas: genomics, biogenesis, mechanism, and function. *Cell*. 2004;116(2):281–297.
13. **Palmieri A**, **Pezzetti F**, **Brunelli G**, **et al**. Differences in osteoblast miRNA induced by cell binding domain of collagen and silicate-based synthetic bone. *J Biomed Sci*. 2007;14(6):777–782.
14. **Sugatani T**, **Hruska KA**. Microrna-223 is a key factor in osteoclast differentiation. *J Cell Biochem*. 2007;101(4):996–999.
15. **Oskowitz AZ**, **Lu J**, **Penfornis P**, **et al**. Human multipotent stromal cells from bone marrow and microRNA: regulation of differentiation and leukemia inhibitory factor expression. *Proc Natl Acad Sci U S A*. 2008;105(47):18372–18377.
16. **Gaur T**, **Hussain S**, **Mudhasani R**, **et al**. Dicer inactivation in osteoprogenitor cells compromises fetal survival and bone formation, while excision in differentiated osteoblasts increases bone mass in the adult mouse. *Dev Biol*. 2010;340(1):10–21.
17. **Kumar J**, **Swanberg M**, **McGuigan F**, **Callreus M**, **Gerdhem P**, **Akesson K**. Lrp4 association to bone properties and fracture and interaction with genes in the WNT- and BMP signaling pathways. *Bone*. 2011;49(3):343–348.
18. **Xu H**, **Duan J**, **Ning D**, **et al**. Role of Wnt signaling in fracture healing. *BMB Rep*. 2014;47(12):666–672.
19. **Einhorn TA**. The Wnt signaling pathway as a potential target for therapies to enhance bone repair. *Sci Transl Med*. 2010;2(42):42ps36.
20. **Furuta T**, **Miyaki S**, **Ishitobi H**, **et al**. Mesenchymal stem cell-derived exosomes promote fracture healing in a mouse model. *Stem Cells Transl Med*. 2016;5(12):1620–1630.
21. **Bao Q**, **Chen S**, **Qin H**, **et al**. An appropriate Wnt/*β*-catenin expression level during the remodeling phase is required for improved bone fracture healing in mice. *Sci Rep*. 2017;7(1):2695.
22. **Kato Y**, **Windle JJ**, **Koop BA**, **Mundy GR**, **Bonewald LF**. Establishment of an osteocyte-like cell line, MLO-Y4. *J Bone Miner Res*. 1997;12(12):2014–2023.
23. TargetScanHuman. 2016. http://www.targetscan.org/vert_71/ (date last accessed 19 July 2021).
24. **Chang MK**, **Kramer I**, **Huber T**, **et al**. Disruption of Lrp4 function by genetic deletion or pharmacological blockade increases bone mass and serum sclerostin levels. *Proc Natl Acad Sci U S A*. 2014;111(48):E5187–E5195.
25. **Zhang Y**, **Liu Y**, **Wu M**, **et al**. MicroRNA-664a-5p promotes osteogenic differentiation of human bone marrow-derived mesenchymal stem cells by directly downregulating HMGA2. *Biochem Biophys Res Commun*. 2020;521(1):9–14.
26. **Chen B**, **Yang W**, **Zhao H**, **et al**. Abnormal expression of miR-135b-5p in bone tissue of patients with osteoporosis and its role and mechanism in osteoporosis progression. *Exp Ther Med*. 2020;19(2):1042–1050.

27. **Kawane T**, **Qin X**, **Jiang Q**, **et al**. Runx2 is required for the proliferation of osteoblast progenitors and induces proliferation by regulating FGFR2 and FGFR3. *Sci Rep*. 2018;8(1):13551.
28. **Wang C**, **Abu-Amer Y**, **O'Keefe RJ**, **Shen J**. Loss of DNMT3B in chondrocytes leads to delayed endochondral ossification and fracture repair. *J Bone Miner Res*. 2018;33(2).
29. **Duvall CL**, **Taylor WR**, **Weiss D**, **Wojtowicz AM**, **Guldberg RE**. Impaired angiogenesis, early callus formation, and late stage remodeling in fracture healing of osteopontin-deficient mice. *J Bone Miner Res*. 2007;22(2).
30. **Saleh S**, **Thompson DE**, **McConkey J**, **Murray P**, **Moorehead RA**. Osteopontin regulates proliferation, apoptosis, and migration of murine claudin-low mammary tumor cells. *BMC Cancer*. 2016;16:359.
31. **Hashemi N**, **Vaezi Z**, **Khanmohammadi S**, **et al**. A novel fluorescent hydroxyapatite based on iron quantum cluster template to enhance osteogenic differentiation. *Mater Sci Eng C Mater Biol Appl*. 2020;111:110775.
32. **Zheng J**, **Zhang X**, **Zhang Y**, **Yuan F**. Osteoblast differentiation of bone marrow stromal cells by femtosecond laser bone ablation. *Biomed Opt Express*. 2020;11(2):885–894.
33. **Lin JC**, **Liu ZG**, **Yu B**, **Zhang XR**. Microrna-874 targeting Sufu involves in osteoblast proliferation and differentiation in osteoporosis rats through the hedgehog signaling pathway. *Biochem Biophys Res Commun*. 2018;506(1):194–203.
34. **Chen Y**, **Yu H**, **Zhu D**, **et al**. miR-136-3p targets PTEN to regulate vascularization and bone formation and ameliorates alcohol-induced osteopenia. *Faseb J*. 2020;34(4):5348–5362.
35. **Lang FM**, **Hossain A**, **Gumin J**, **et al**. Mesenchymal stem cells as natural biofactories for exosomes carrying miR-124a in the treatment of gliomas. *Neuro Oncol*. 2018;20(3):380–390.
36. **Jia Y**, **Qiu S**, **Xu J**, **Kang Q**, **Chai Y**. Exosomes secreted by young mesenchymal stem cells promote new bone formation during distraction osteogenesis in older rats. *Calcif Tissue Int*. 2020;106(5):509–517.
37. **Chen X**, **Shi Y**, **Xue P**, **Ma X**, **Li J**, **Zhang J**. Mesenchymal stem cell-derived exosomal microRNA-136-5p inhibits chondrocyte degeneration in traumatic osteoarthritis by targeting ELF3. *Arthritis Res Ther*. 2020;22(1):256.
38. **Ivey KN**, **Srivastava D**. microRNAs as developmental regulators. *Cold Spring Harb Perspect Biol*. 2015;7(7):a008144.
39. **Xie S**, **Li X**, **Qian L**, **et al**. An integrated analysis of mRNA and miRNA in skeletal muscle from myostatin-edited Meishan pigs. *Genome*. 2019;62(5):305–315.
40. **Wang C**, **Zhang Z**, **Zhang H**, **et al**. Susceptibility genes for osteoporotic fracture in postmenopausal Chinese women. *J Bone Miner Res*. 2012;27(12):2582–2591.
41. **Bukowska-Olech E**, **Sowinska-Seidler A**, **Szczaluba K**, **Jamsheer A**. A novel biallelic splice-site variant in the LRP4 gene causes sclerosteosis 2. *Birth Defects Res*. 2020;112(9):652–659.
42. **Zheng C**, **Qu Y-X**, **Wang B**, **Shen P-F**, **Xu J-D**, **Chen Y-X**. Cox-2/Pge2 facilitates fracture healing by activating the Wnt/β-catenin signaling pathway. *Eur Rev Med Pharmacol Sci*. 2019;23(22):9721–9728.

Author information:
- H. Yu, MD, Associate Professor
- J. Zhang, MM, Attending Doctor
- X. Liu, MD, Associate Professor
- Y. Li, MD, Associate Professor

Department of Orthopedics, The Second Hospital of Jilin University, Changchun, China.

Author contributions:
- H. Yu: Conceptualization.
- J. Zhang: Formal analysis, Writing – original draft, Writing – review & editing.
- X. Liu: Formal analysis, Writing – original draft.
- Y. Li: Investigation, Writing – original draft, Writing – review & editing.

Funding statement:
- No benefits in any form have been received or will be received from a commercial party related directly or indirectly to the subject of this article.

Acknowledgements:
- We sincerely thank the technical support of central laboratory of Jilin University.

Open access funding
- The authors confirm that the open access fee for this study was self-funded.